

Experimental Study on the Residual Strength of Coal Under Low Confinement

Fuqiang Gao^{1,2} · Hongpu Kang^{1,2}

Received: 26 January 2016 / Accepted: 17 October 2016 / Published online: 21 October 2016
© Springer-Verlag Wien 2016

Abstract In underground coal mining, coal rib failure of longwall entries is almost certain due to the relative weakness of coal and the presence of high mining-induced stresses. To maintain the coal's capability of sustaining large loads after failure and substantial deformation, it is crucial to understand its post-peak behavior and subsequently, its residual strength. In this study, triaxial compression tests were performed on a total of 51 coal specimens that were classified into two groups based on the existence of calcite grains. Particular emphasis was given to evaluating the residual strength of the coal specimens. It was found that the presence of calcite grains has significant effect on the brittleness of the coal. Coal specimens containing calcite grains have lower frictional strength than specimens without calcite grains. The tests demonstrated that splitting is completely suppressed when the confinement exceeds 10 % of the coal's unconfined compressive strength. The Coulomb and Hoek–Brown failure criteria satisfactorily fit the coals' peak strength data over the entire confining stress range. The Hoek–Brown failure criterion satisfactorily fits the residual strength data. The parameter m for residual strength is significantly greater than that of the peak strength for both groups of coal. It was also found that as the confinement increases, the increase in residual strength is greater than the increase in peak strength.

Keywords Confined compressive strength · Residual strength · Failure mechanism · Coal

1 Introduction

In mining, the formation of post-peak failure regions around underground structures is sometimes unavoidable (Tutluoğlu et al. 2014). The optimal design of structures (i.e., pillars and drifts) is based not only on peak strength, but also on post-peak behavior and thus on residual strength. This is particularly true in underground coal mining for two reasons: (1) coal mine openings are excavated in Coal Measure rocks, which have relatively weak strengths and (2) these openings usually suffer mining-induced stresses that can reach up to six times the overburden stress, σ_o . $\sigma_o = \gamma h$, where h is the mining depth and γ is the weighted average unit weight of the overburden strata (Peng 1986). Under such significant mining-induced stresses, the Coal Measures rock will unavoidably fail, yielding considerable plastic deformation and reaching its residual strength. This unstable situation is particularly applicable to longwall entries. Longwall entries are usually excavated in coal seams which are normally the weakest structures in Coal Measures. The primary concern in Chinese coal mining ground control practices is often not roof collapses, but rather the extreme coal rib failure caused by mining-induced pressures, as seen in Fig. 1. Severe rib-to-rib convergence can block necessary escape routes and ventilation airways. Blocked ventilation airways could cause gob combustion, an extremely hazardous and impermissible outcome. For coal mining using the room-and-pillar method, coal pillars usually have modest to large width to height ratios, and when subjected to extreme loading, could undergo complex processes of progressive failure.

✉ Fuqiang Gao
fuqgao@gmail.com

¹ State Key Laboratory of Coal Mining and Clean Utilization, China Coal Research Institute, Beijing, China

² Mining and Designing Branch, China Coal Research Institute, Beijing, China

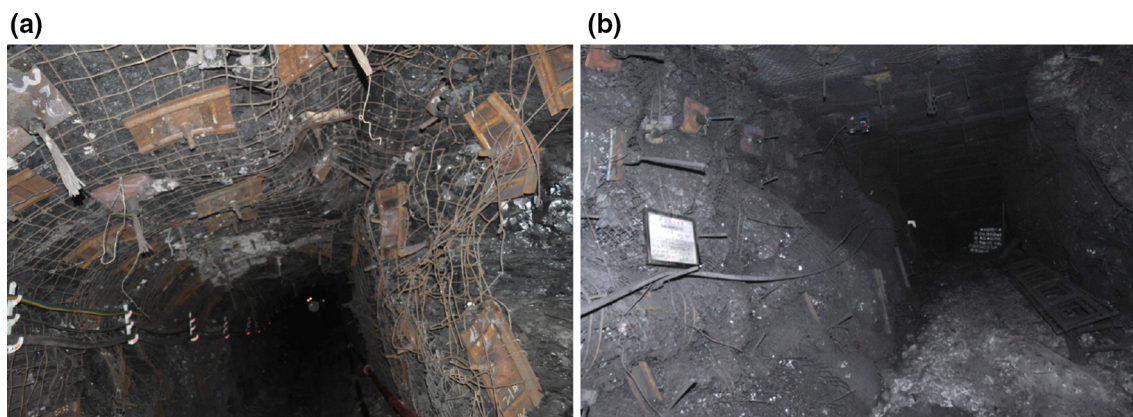
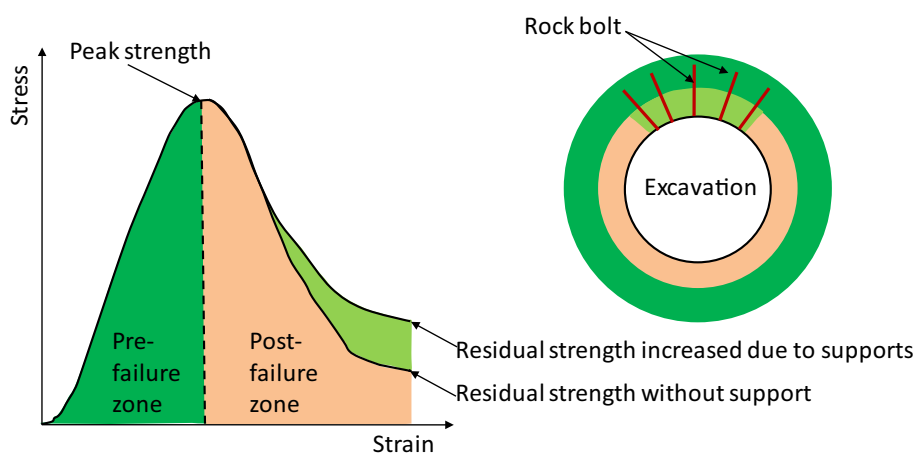


Fig. 1 Examples of highly fractured coal around underground mine roadways

Fig. 2 Relationship of complete stress–strain curve on rock excavation work (modified after Hudson 1989)



When coal failure is unavoidable, coal mine engineers' main concerns becomes the residual strength and support methods needed to increase the coal's residual strength so that the failed coal can maintain its capacity to sustain large loads after substantial deformation, see Fig. 2. In this case, knowing the residual strength and deformation characteristics of failed coal is even more important than knowing its peak strength. Cai et al. (2007) investigate the influence of the residual strength on the yielding zone around a tunnel by means of numerical modeling. The rock was assumed to reach its residual strength in a brittle manner after reaching its peak strength. The numerically predicted excavation-induced damage varied drastically based on different residual strengths even though the peak strength was identical throughout. Knowing the residual strength is therefore crucial to achieving a stable structure and an optimal rock support design.

Many tests have been conducted on coal specimens from the laboratory scale to the large (i.e., 1.5 m) scale to investigate the strength and deformation characteristics of coal (Bieniawski 1968a, b; Medhurst and Brown 1998; Zuo et al. 2011; Buzzzi et al. 2014; Peng et al. 2014). Most of these studies, however, focused on the peak strength of

coal, and only a few studies focused on the residual strength. In this study, a series of tests were performed on laboratory coal specimens to investigate their strength and deformation characteristics, with particular interest in the coals' post-peak behavior and residual strengths.

2 Description of the Coal

The coal used in the study was obtained from block cutting in the #5 coal seam at the 50103 longwall panel in the Hejiata Coal Mine, China, see Fig. 3. The thickness of the coal seam ranged from 2.4 to 3.8 m. The coal contains 5.56–10.38 % ash and 8.29–9.14 % moisture.

Calcite grains were observed as “gray spots” in parts of the coal. To evaluate the influence of the calcite grains on the mechanical behavior of the coal, two groups of coal specimen were prepared for the present study: Group 1 with calcite grains and Group 2 without calcite grains, see Fig. 4. Since specimen-scale structures (i.e., cleats, defects) were observed in all the tested specimens, the specimens could not be regarded as “intact” coal. One thin section from each of the two groups of coal was prepared to

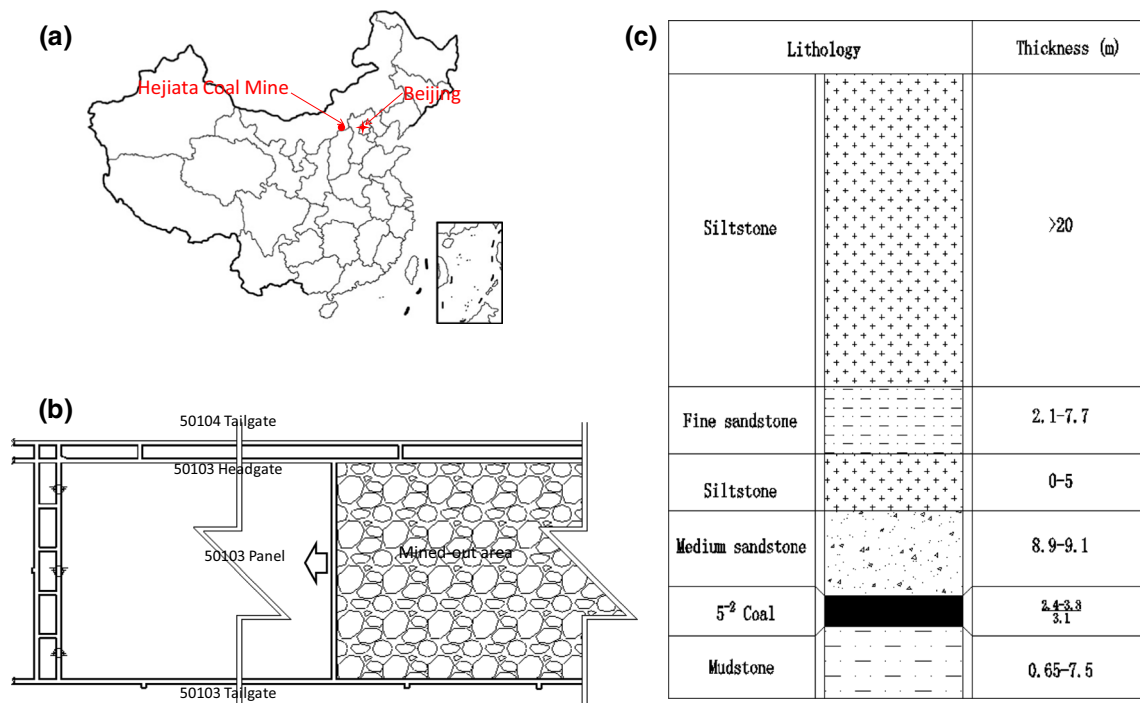


Fig. 3 **a** Location of the Hejiata Coal Mine, **b** layout of the longwall panel from where coal blocks were obtained and **c** lithology of the longwall panel

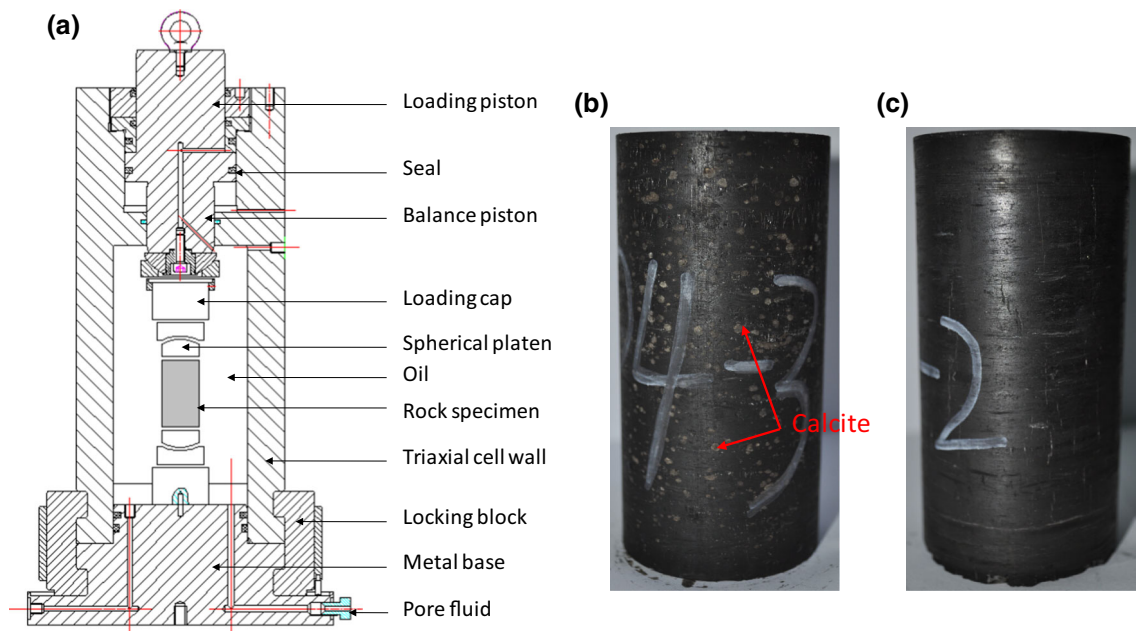


Fig. 4 Triaxial compression test apparatus and examples of coal specimens used in this study. **a** Schematic of the apparatus, **b** Group 1 specimen with calcite structure and **c** Group 2 without calcite structure

determine the coals’ petrographic characteristics. The mineralogical content of the coal was determined semi-quantitatively using X-ray diffraction, see Fig. 5, which confirms that the “gray spots” are calcite grains. An optical polarizing microscope was used to determine the average size and modal composition of the calcite grains. Figure 6

shows petrographic images of the coal containing calcite grains. The microstructure and mineralogy composition of the coal were observed by reflected light microscopy with oil-immersion lens, see Fig. 7. In Group 1, calcite grains were dominant with a volume percent of approximately 26 % and their size ranged from 100 μm to 3 mm. Fusinite

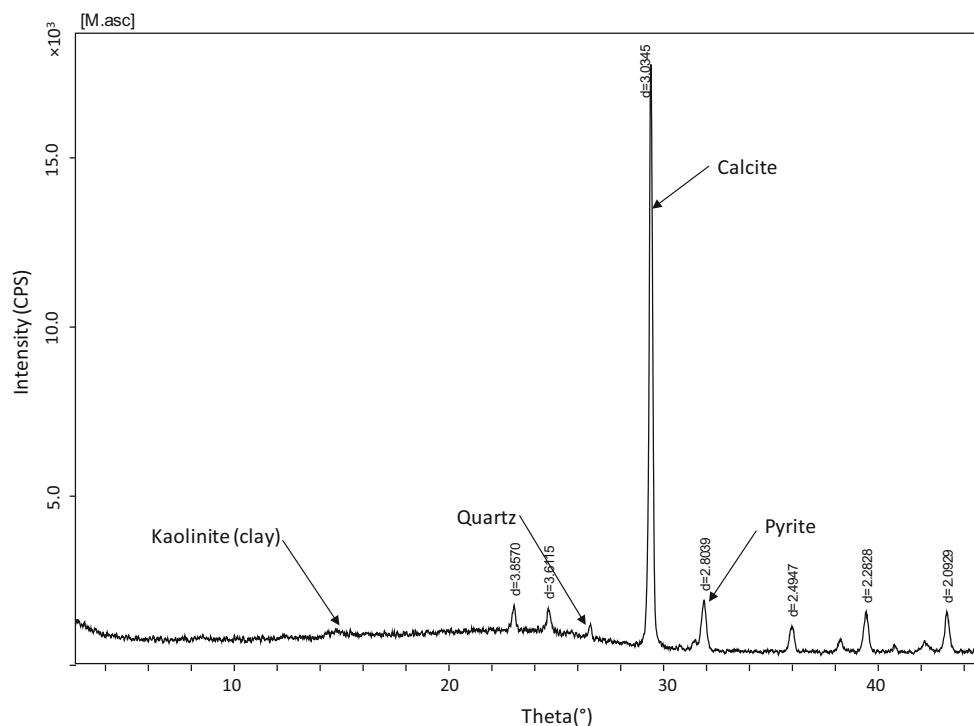


Fig. 5 X-ray diffraction pattern of the coal containing calcite grains

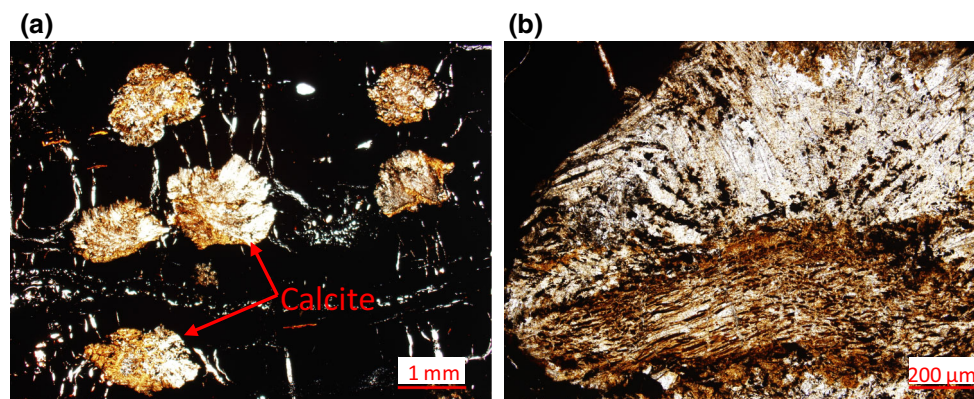


Fig. 6 Reflected light microscopy analysis on thin sections of coal specimens containing calcite grains

and pyrite were identified; the size of the fusinite ranged from 0.5 to 20 μm , and the size of exinite ranged from 0.1 to 10 μm . The density of the Group 1 and 2 was 1.495 and 1.298 g/mm^3 , respectively.

3 Sampling and Testing Methods

3.1 Sampling, Specimen Characterization and Specimen Handling

ISRM (1979) suggests that the ratio of specimen diameter to the size of the largest grain should be greater than 10:1.

Coal cannot be characterized by a particular grain size since it contains more macerals (fibers) than minerals (grains). In Group 1 specimens containing calcite grains, the maximum size of the calcite grains was approximately 3 mm. Accordingly, the specimen diameter should be more than 30 mm. In the present study, all the specimens were cylindrical, 50 mm in diameter and 100 mm in length.

The specimens were cored with the bedding planes perpendicular to the long axis. The ends of the specimen were carefully surfaced using a rotating grinding device. The specimens were jacketed with 3-mm-thick soft rubber to prevent pressure fluid from entering porous rock specimens.

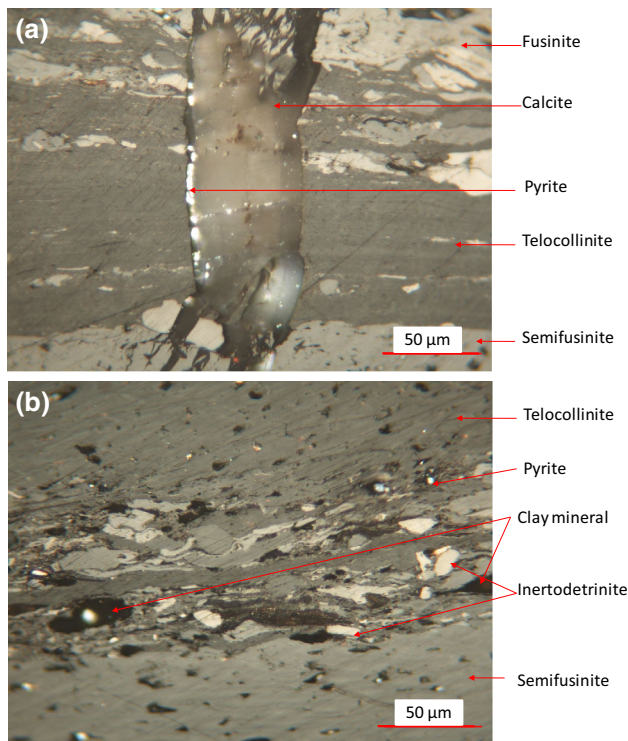


Fig. 7 Reflected light microscopy with oil-immersion analysis on thin sections of coal specimens. **a** Group 1 specimen with calcite structure and **b** Group 2 without calcite structure

3.2 Testing Procedure

The tests were conducted generally according to the ISRM suggested method for determining the strength of rock in confined compression (ISRM 1979). The specimens were loaded on a digital servo-controlled testing machine with a 3000 kN capacity, see Fig. 4a.

Throughout the test, the confining pressure in the triaxial vessel was maintained at a predetermined value. The confining stress levels were chosen to simulate the range of confining stresses relevant to underground excavations at the Hejiata coal mine and to enable investigation of the transition from axial splitting failure to macroscopic shear failure. The following two aspects were considered for defining the confining stress range: (1) stress measurements conducted in the Hejiata coal mine suggest that the minimum horizontal stress is 5.44 MPa; considering the stability of the coal surrounding a roadway, the maximum confinement applied on the roadway ribs would be approximately 5 MPa. (2) Former experimental results suggest that the brittle-to-ductile transition takes place when the confining pressure is between 3.0 and 4.0 MPa. Based on these considerations, the tests were performed with a range of confining stress from 0 to 5 MPa, which covers the possible confining pressures experienced by the

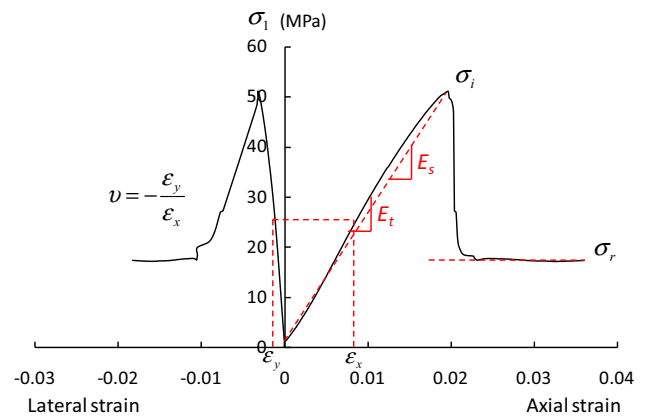


Fig. 8 Determination of tangent Young's modulus, E_t , secant Young's modulus, E_s , peak strength σ_i , Poisson's ratio ν and residual strength σ_r from complete axial stress–axial strain curve of compression test

coal in field and causes the coal to fail in different failure patterns from brittle to ductile.

Two cylindrical platens incorporating a spherical seating were placed between the machine and the specimen, see Fig. 4a. The purpose of the spherical seat is to provide a uniform axial stress distribution on the specimen. The axial stress was applied perpendicularly to the bedding planes. To capture stable post-peak failure behavior of the brittle coal specimens and to achieve the transition from peak to residual strength, the axial load was applied at a small constant strain rate of $10\text{--}5\text{ s}^{-1}$. The load was stopped when a stress plateau with little or no drop in the stress was observed after the peak. The specimens' strains were determined by displacement measurements using axial and lateral displacement transducers. A test was considered to be valid only when a complete axial stress–axial strain curve was obtained. Mechanical properties of the specimen were then derived from the axial stress–axial strain curve, as shown in Fig. 8. The residual strength was defined by the plateau, in a strain range of about 2–4 times the strain corresponding to the peak strength. A total of 21 Group 1 specimens and 30 Group 2 specimens were tested in this study.

4 Compression Test Results

4.1 Deformation Behavior of the Coal Specimens

The results of all specimens tested in the present study are summarized in Table 1. The tangent Young's modulus, E_t , is determined as the slope of the axial stress–axial strain curve at 50 % of the peak strength and the secant Young's modulus, E_s , is the slope of a straight line joining the origin of the axial stress–axial strain curve to the point of peak

Table 1 Summary of test results for coal specimens

Specimen no.	E_t (GPa)	E_s (GPa)	ν	σ_3 (MPa)	σ_l (MPa)	σ_r (MPa)	σ_r/σ_l	Failure pattern
P0-1	3.6	3.1	0.20	0.0	31.0	N/A	N/A	A
P0-2	3.4	3.1	0.28	0.0	37.1	N/A	N/A	A
P0-3	3.0	2.9	0.27	0.0	39.6	N/A	N/A	A
P0-4	2.8	2.7	0.27	0.0	31.9	N/A	N/A	A
P1-1	3.0	2.8	0.29	0.5	44.0	12.0	0.27	A
P1-2	3.8	3.3	0.30	0.5	40.2	11.7	0.29	M
P1-3	3.1	3.0	0.31	0.5	30.5	9.0	0.30	A
P1-4	3.1	2.8	0.29	0.5	43.5	10.5	0.24	A
P2-1	3.4	2.9	0.26	1.0	48.7	9.0	0.18	M
P2-2	3.5	2.9	0.26	1.0	42.4	14.1	0.33	A
P2-3	3.7	3.1	0.37	1.0	45.5	10.6	0.23	A
P2-4	2.8	2.6	0.35	1.0	41.5	13.5	0.33	A
P3-1	3.4	3.0	0.33	2.0	43.2	16.3	0.38	S
P3-2	3.1	2.7	0.27	2.0	51.4	18.0	0.35	M
P3-3	3.3	2.8	0.37	2.0	50.4	18.2	0.36	S
P3-4	2.9	2.6	0.35	2.0	54.0	24.4	0.45	M
P4-1	3.6	3.0	0.38	3.5	54.0	25.7	0.48	S
P4-2	4.2	3.0	0.25	3.5	50.0	24.3	0.49	S
P4-3	3.5	2.7	0.11	3.5	58.5	25.8	0.44	S
P5-1	3.8	2.8	0.32	5.0	48.3	32.0	0.66	M
P5-2	3.2	2.4	0.21	5.0	56.8	25.0	0.44	S
P5-3	3.5	2.6	0.25	5.0	62.4	29.9	0.48	S
S0-1	1.9	1.8	0.23	0.0	28.3	N/A	N/A	A
S0-2	2.0	2.0	0.26	0.0	42.4	N/A	N/A	A
S0-3	2.4	2.4	0.28	0.0	43.9	N/A	N/A	A
S0-4	2.1	1.7	0.27	0.0	27.7	N/A	N/A	A
S0-5	2.1	2.1	0.28	0.0	42.5	N/A	N/A	A
S1-1	2.4	2.4	0.30	0.5	45.7	7.4	0.16	A
S1-2	2.4	2.2	0.30	0.5	41.3	8.3	0.20	A
S1-3	2.7	2.6	0.36	0.5	36.4	8.6	0.24	A
S1-4	2.6	2.5	0.32	0.5	40.7	7.5	0.18	A
S1-5	2.3	2.0	0.30	0.5	34.6	7.7	0.22	A
S2-1	2.5	2.5	0.31	1.0	39.7	12.0	0.30	A
S2-2	2.5	2.5	0.30	1.0	49.5	11.5	0.23	M
S2-3	2.3	2.0	0.30	1.0	42.0	11.8	0.28	M
S2-4	2.2	2.1	0.29	1.0	33.4	13.5	0.40	M
S2-5	2.6	2.6	0.34	1.0	51.8	10.0	0.19	M
S3-1	2.6	2.5	0.17	2.0	49.7	16.0	0.32	M
S3-2	2.4	2.2	0.30	2.0	46.8	20.0	0.43	M
S3-3	2.5	2.3	0.31	2.0	49.9	16.4	0.33	M
S3-4	2.4	2.4	0.30	2.0	55.0	18.0	0.33	M
S3-5	2.8	2.8	0.35	2.0	62.5	14.5	0.23	M
S4-1	3.1	2.9	0.30	3.5	57.1	17.0	0.30	S
S4-2	2.9	2.9	0.40	3.5	53.5	23.8	0.44	S
S4-3	2.3	2.1	0.27	3.5	60.3	21.5	0.36	S
S4-4	2.4	2.3	0.30	3.5	70.3	28.0	0.40	S
S4-5	2.8	2.8	0.35	3.5	61.4	20.8	0.34	S
S5-1	2.6	2.6	0.34	5.0	64.5	23.4	0.36	S

Table 1 continued

Specimen no.	E_t (GPa)	E_s (GPa)	ν	σ_3 (MPa)	σ_l (MPa)	σ_r (MPa)	σ_r/σ_l	Failure pattern
S5-2	2.8	2.8	0.35	5.0	72.3	22.8	0.32	S
S5-3	2.5	2.4	0.31	5.0	67.3	30.5	0.45	S
S5-4	2.5	2.4	0.34	5.0	53.7	31.3	0.58	S
S5-5	2.9	2.8	0.36	5.0	59.5	26.0	0.44	S

E_t = tangent Young's modulus, E_s = secant Young's modulus, ν = Poisson's ratio, σ_3 = confining stress, σ_l = peak strength, σ_r = residual strength, A = axial splitting, S = shear bands, M = mixed splitting and shear bands

Fig. 9 Effect of confining pressure on the deformation behavior of the coal specimens. **a** Tangent Young's modulus, **b** secant Young's modulus

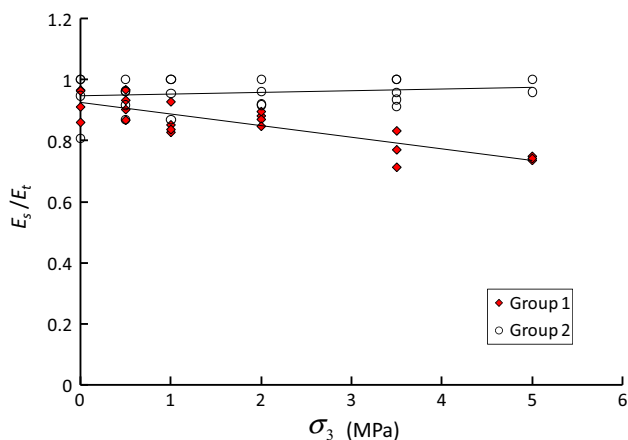
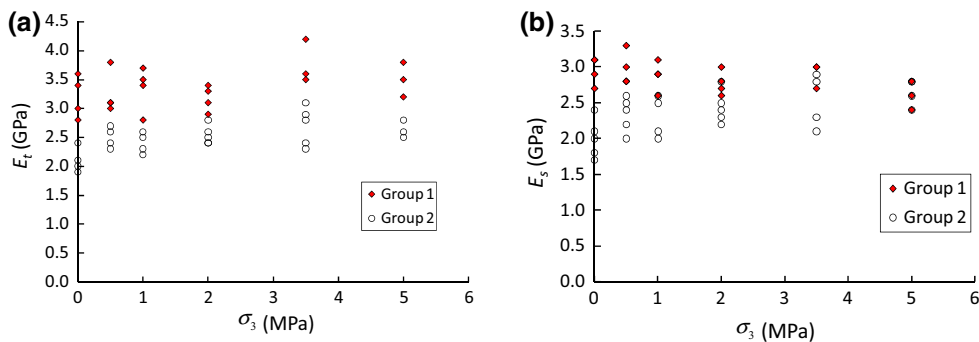


Fig. 10 Effect of confining pressure on the E_s/E_t

stress. Figure 9 shows the E_t and E_s of all coal specimens tested at varying confining pressures. It can be seen that both the E_t and E_s display a significant range of values at each confining pressure. Both the E_t and E_s values obtained from Group 1 specimens containing calcite grains are generally greater than those from the Group 2 specimens. This can be attributed to the relatively low deformability of calcite in comparison with the coal. The structure and mineralogy composition might also play a role in this phenomenon. The two groups of the tested coal specimens were obtained from the same coal seam, more specifically, by cutting the same coal block. Thus, it would be reasonable to suggest that the major difference of the deformability between the two groups is the presence of calcite

grains. The confining pressure appears to have no major influence on either E_t or E_s over the range considered.

To compare E_t and E_s , the E_s/E_t ratio was plotted against the confining pressure (Fig. 10). For the Group 1 specimens, the values of E_s/E_t vary between 0.71 and 0.97, with an average value of 0.86. The E_s/E_t ratio appears to decrease with confining pressure. For the Group 2 specimen, the values of E_s/E_t vary between 0.81 and 1.0, with an average value of 0.96, independent of confining pressure. The Group 1 specimen exhibited a greater difference between E_s and E_t than the Group 2 specimen. This is because the Group 1 specimen containing calcite grains exhibited a distinct nonlinear behavior prior to the peak strength (Fig. 11a). This nonlinear behavior was not distinct for the Group 2 specimen without calcite grains (Fig. 11b). It is also interesting to note that the post-peak behavior of the Group 2 specimen was more brittle than that of the Group 1 specimens, indicating that the existence of calcite grains restrained the brittleness of the coal. Figure 10 also shows that the confining pressure has a substantial influence on the secant Young's modulus of Group 1 but limited influence on Group 2 over the confinement range considered.

4.2 Peak Strengths and Failure Mechanisms of the Coal Specimens

Figure 12 shows the peak strength plotted against the confining pressure for all the tested coal specimens. For both Group 1 and 2 specimens, the test results yielded a significant range of peak strengths at each confining

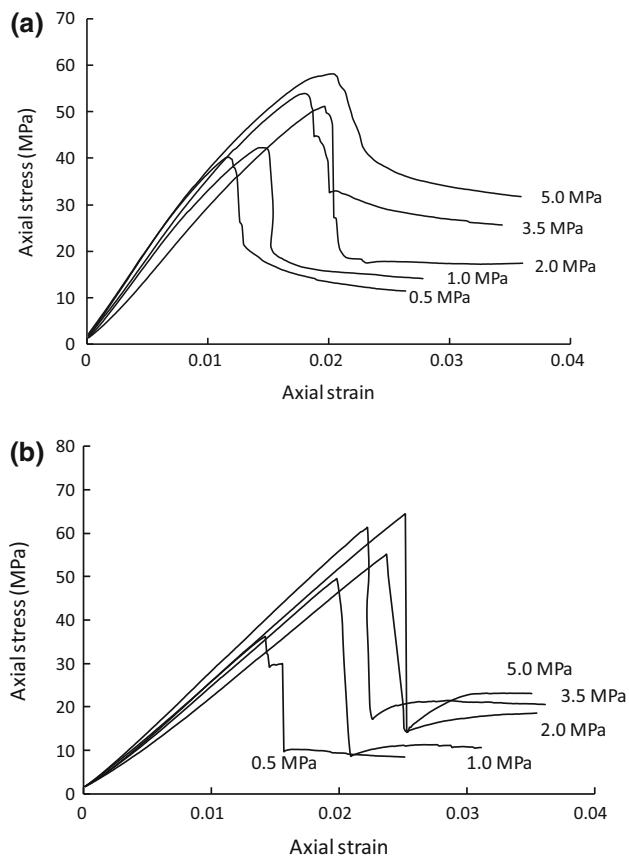


Fig. 11 Axial stress–strain behavior of coal specimens under varying confining pressures. **a** Group 1 specimens, **b** Group 2 specimens

pressure. It is hypothesized that such variability in peak strength is due to the microstructure variability and the specimen-scale structures including cleats and defects within the coal specimens.

It is known that coal specimens exhibit different failure mechanisms when under compression, depending on the confining pressure. Medhurst and Brown (1998) characterized two identifiable failure mechanisms in coal specimens subjected to compression: axial splitting at low confining pressures and shear bands at high confining pressures. Buzzi et al. (2014) suggested that coal may exhibit mixed splitting and shear band patterns at intermediate confining pressures. In the present study, three different failure mechanisms were observed for the tested specimens under varying confining pressures. At low confining pressures (≤ 1 MPa), axial splitting was generally observed (Figs. 13a, 14a). Mixed splitting and shear band patterns were generally observed when the confining pressure was between 1 and 2 MPa (Figs. 13b, 14b). At relatively high confining pressures (3.5–5.0 MPa), nearly all the tested specimens failed in shear bands, except one of

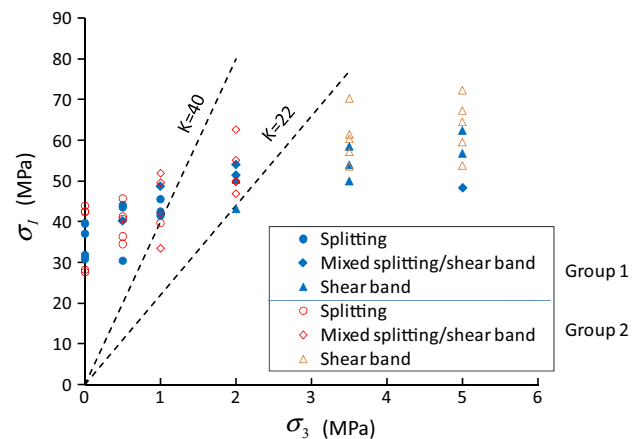


Fig. 12 Peak strength versus confining pressure for all coal specimens under compressions. K is spalling limit defined as $K = \sigma_1/\sigma_3$

the Group 1 specimens that failed in mixed splitting and shear bands (Figs. 13c, 14c).

When subjected to compression, rock-like materials exhibit a transition from axial splitting to macroscopic shear failure as the confining pressure increases. Kaiser and Kim (2014) use the spalling limit (principal stress ratio σ_1/σ_3) to describe the transition threshold and suggest that the spalling limit is between 10 and 20 for hard rocks. For all the coal specimens tested in the present study, the spalling limit was approximately 40. This value was very close to the spalling limit of an Australian coal at 38 (Buzzi et al. 2014). The spalling limit of the coal appears to be much greater than that of hard rock, implying that axial splitting can be suppressed by relatively low confinement in contrast to hard rocks. If evaluating the threshold between mixed failure and shear bands, the spalling limit of the coal was approximately 22, which was consistent with hard rocks. Splitting was totally suppressed when the confinement was greater than 3.5 MPa, corresponding to around 10 % of the unconfined compression strength of the tested coal.

4.3 Residual Strengths of the Coal Specimens

The residual strength of each tested coal specimen was obtained. Figure 15 shows the residual strength plotted against the confining pressure for all the tested coal specimens under confined condition. All the specimens under unconfined conditions exhibited no residual strength after failure and therefore are not taken into account in this analysis. For both Group 1 and 2 specimens, the residual strengths are significantly scattered at each confining pressure. Generally, the residual strength increases with confining pressure. The influence of the confinement on the residual strength of coal was further evaluated by comparing

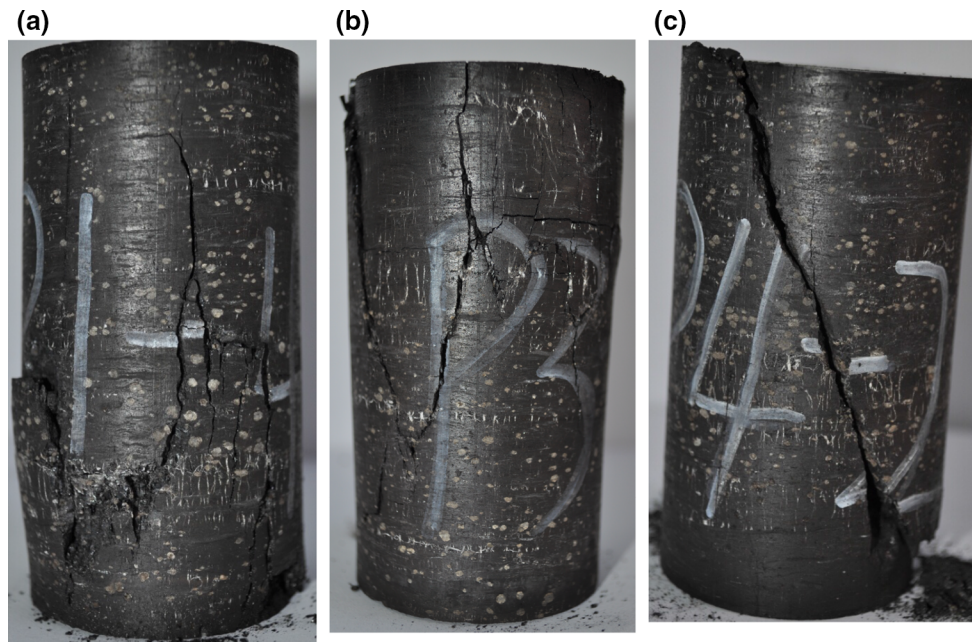


Fig. 13 Three types of failure patterns observed in Group 1 coal specimens under different confinements. **a** Axial splitting ($\sigma_3 = 0.5$ MPa), **b** mixed axial splitting and shear band ($\sigma_3 = 2.0$ MPa), **c** shear band ($\sigma_3 = 5.0$ MPa)

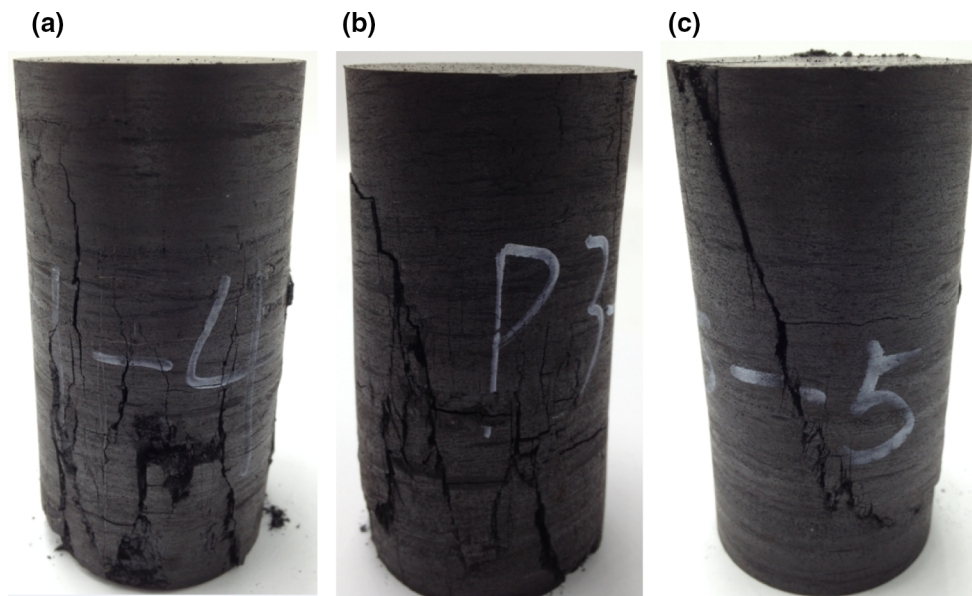


Fig. 14 Three types of failure patterns observed in Group 2 coal specimens under different confinements. **a** Axial splitting ($\sigma_3 = 0.5$ MPa), **b** mixed axial splitting and shear band ($\sigma_3 = 2.0$ MPa), **c** shear band ($\sigma_3 = 3.5$ MPa)

the residual strength to the peak strength. It is clear from Fig. 16 that the residual strength to peak strength ratio increases with confinement. In other words, as the confinement increases, the increase in residual strength is greater than the increase in peak strength. This finding is consistent with field observations in underground coal pillars, where the residual strength to peak strength ratio increases with distance into the pillar (Li and Heasley 2014), see Fig. 17.

4.4 Failure Criteria

4.4.1 Peak Strength

Two strength models, the linear Coulomb criterion and the nonlinear Hoek–Brown criterion were used to characterize the failure envelope of the tested coal specimens. The Coulomb criterion is described as (Labuz and Zang 2012):

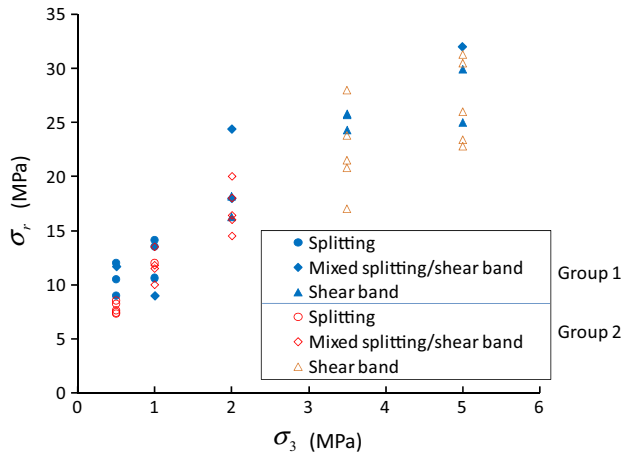


Fig. 15 Residual strength versus confining pressure for all coal specimens under confined compressions

$$(\sigma_1 - \sigma_3) = (\sigma_1 + \sigma_3) \sin \phi + 2c \cos \phi \quad (1)$$

where σ_1 and σ_3 are the maximum and minimum principal stresses at failure, respectively, and c and ϕ are two material constants, cohesion and internal friction angle, respectively.

The generalized Hoek–Brown failure criterion simplifies to (Hoek et al. 2002)

$$\sigma_1 = \sigma_3 + \sigma_{ci} \left(m_i \frac{\sigma_3}{\sigma_{ci}} + 1 \right)^a \quad (1)$$

where σ_{ci} is the unconfined compressive strength and m_i is a material constant reflecting the frictional and dilational behavior of the rock. The power a is assumed to be constant at 0.5 in the present study.

The two Hoek–Brown parameters can be determined by statistical analysis of the triaxial compression test data. A Levenberg–Marquardt nonlinear regression method was used to derive the parameters for the peak strength of the tested coal specimens. The equivalent Coulomb parameters were also determined. The derived parameters for the peak strength are listed in Table 2. The tested data and the resulting fits are plotted in Fig. 18.

Both the Coulomb and Hoek–Brown failure criteria appear to satisfactorily fit the data over the entire confining stress ranges of the Group 1 and Group 2 specimens. The m_i and the internal friction angle ϕ of the Group 2 specimens are 12.6° and 44.4°, respectively, much greater than the 8.0° and 37.8° of the Group 1 specimens, indicating that the frictional strength of the coal without calcite grains is higher than that of the coal containing calcite grains.

4.4.2 Residual Strength

As discussed previously, the examination on the failure patterns of the coal specimens shows that shear failure

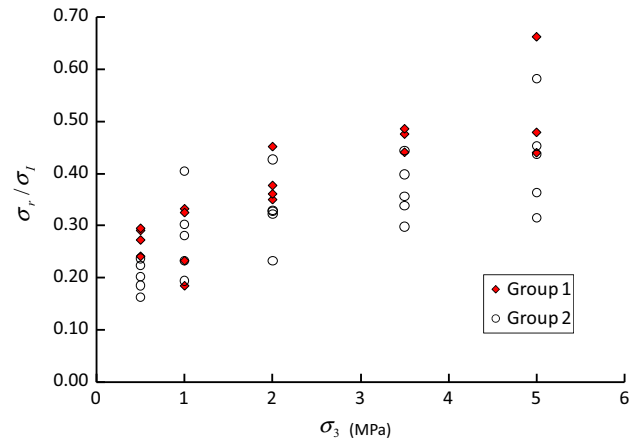


Fig. 16 Residual strength and peak strength ratio of all specimens under varying confining pressures

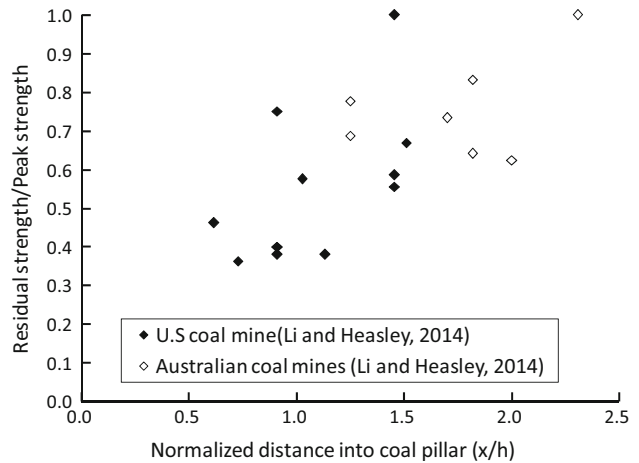


Fig. 17 Variations of residual strength to peak strength ratio as a function normalized distance into pillar for coal. x and h refer to the distance into pillar and pillar height, respectively

Table 2 Parameters in generalized Hoek–Brown peak compressive strength criterion and Mohr–Coulomb peak compressive strength criterion

	σ_i (MPa)	m_i	$\sum e^2$
Group 1	37.6	8.0	516
Group 2	37.2	12.6	1180
	c (MPa)		ϕ (°)
Group 1	9.4		37.8
Group 2	8.0		44.4

$\sum e^2$ = error sum of squares

plays a dominant role. This is more pronounced under the conditions of relatively high confining pressures (i.e., 3.5–5.0 MPa). When a coal specimen reaches its residual strength and sliding on a failure plane takes place, it can be

Fig. 18 Peak strength criteria for coal specimens. **a** Group 1, **b** Group 2

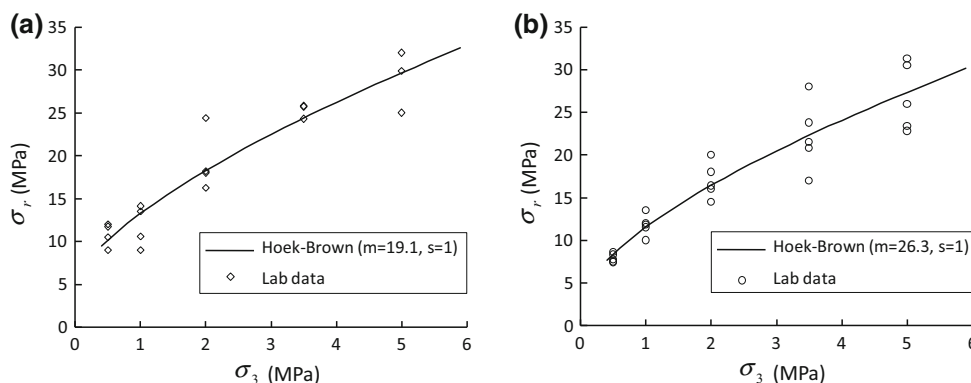
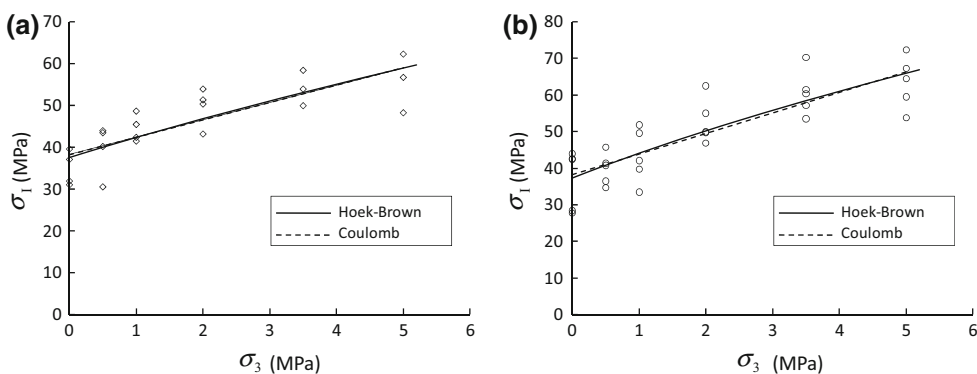


Fig. 19 Measured and predicted residual strength of coal specimens subjected to confined compression. **a** Group 1, **b** Group 2

Table 3 Parameters in generalized Hoek–Brown residual compressive strength criterion

	$\sigma_r(\text{MPa})$	m_r	$\sum e^2$
Group 1	6.0	19.1	106
Group 2	3.7	26.3	157

$\sum e^2$ = error sum of squares

conservatively assumed that all cohesive strength across the failure plane is lost and that the only resistance to the applied loads is provided by the friction along the failure plane. The roughness or dilatancy of the failure plane should be considered in contributing to sliding friction, which further complicates the interpretation of the relationship between residual strength and confining pressure. As suggested by some researchers (Cai et al. 2007; Karam and Tabbara 2009; Walton et al. 2014), the Hoek–Brown criterion might be appropriate for describing the relationship between residual strength and confining pressure. Figure 19 plots the Hoek–Brown strength criterion which was derived using the residual strength data. The derived Hoek–Brown parameters are listed in Table 3. Note that only those specimens under confined condition were taken into account in this analysis. The specimens under unconfined conditions did not sustain any load after failure

(i.e., no residual strength) and thus were not taken into account when examining the relationship between residual strength and confining pressure. For both Group 1 and Group 2 coal specimens, the Hoek–Brown failure criterion appears to satisfactorily fit the residual strength data. In addition, for both Group 1 and Group 2 coal specimens, the derived residual strength parameter m_r is significantly greater than that of the peak strength, implying that the frictional component strength plays a dominant role in the post-peak behavior of the coal.

5 Conclusions

The underground coal mining industry faces the challenge of severe coal rib damage as mining activity advances to greater depths. To maintain failed coal’s capability of sustaining large loads after substantial deformation, it is crucial to know the coal’s residual strength. Understanding the residual strength will enable mining engineers to achieve a stable structure and an optimal rock support design. In this study, unconfined and confined compression tests were conducted on a total of 51 coal specimens that were classified into two groups based on the existence of calcite grains. The compression tests were carried out under relatively low confinement (0–5.0 MPa). Particular

emphasis was placed on the evaluation of the residual strength of the coal specimens.

It was found that confining pressure has no major influence on the Young's modulus of the coal. The coal specimens containing calcite grains were found to have lower frictional strength than the specimens without calcite grains.

Three types of failure modes were observed in the tested coal specimens under low confinement, splitting, mixed splitting and shear bands. Splitting was totally suppressed when the confinement exceeded 10 % of the coal's unconfined compressive strength. The Coulomb and Hoek–Brown failure criteria can satisfactorily fit the data of the peak strengths of the coal over the entire confining stress range. Hoek–Brown can satisfactorily fit the data of residual strength. The parameter m for residual strength is significantly greater than that of the peak strength for both groups of coal. As the confinement increases, the increase in residual strength is greater than the increase in peak strength.

Acknowledgments This work has been supported by the National Natural Science Foundation of China (Grant Nos. U1261211, 51304119).

References

- Bieniawski ZT (1968a) The effect of specimen size on compressive strength of coal. *Int J Rock Mech Min Sci Geomech Abstr* 5:325–335. doi:[10.1016/0148-9062\(68\)90004-1](https://doi.org/10.1016/0148-9062(68)90004-1)
- Bieniawski ZT (1968b) In situ strength and deformation characteristics of coal. *Eng Geol* 2:325–340. doi:[10.1016/0013-7952\(68\)90011-2](https://doi.org/10.1016/0013-7952(68)90011-2)
- Buzzi O, Sieffert Y, Mendes J et al (2014) Strength of an Australian coal under low confinement. *Rock Mech Rock Eng*. doi:[10.1007/s00603-013-0493-5](https://doi.org/10.1007/s00603-013-0493-5)
- Cai M, Kaiser PK, Tasaka Y, Minami M (2007) Determination of residual strength parameters of jointed rock masses using the GSI system. *Int J Rock Mech Min Sci* 44:247–265. doi:[10.1016/j.ijrmms.2006.07.005](https://doi.org/10.1016/j.ijrmms.2006.07.005)
- Hoek E, Carranza-Torres C, Corkum B (2002) Hoek–Brown failure criterion—2002 edition. In: *Proceedings of NARMS-TAC 2002 conference*. Toronto, pp 267–273
- Hudson JA (1989) *Rock mechanics principles in engineering practice*. Butterworth-Heinemann, London
- ISRM (1979) Suggested methods for determining the uniaxial compressive strength and deformability of rock materials. *Int J Rock Mech Min Sci Geomech Abstr* 16:102. doi:[10.1016/0148-9062\(79\)90262-6](https://doi.org/10.1016/0148-9062(79)90262-6)
- Kaiser PK, Kim B-H (2014) Characterization of strength of intact brittle rock considering confinement-dependent failure processes. *Rock Mech Rock Eng*. doi:[10.1007/s00603-014-0545-5](https://doi.org/10.1007/s00603-014-0545-5)
- Karam G, Tabbara M (2009) Hoek–Brown strength criterion for actively confined concrete. *J Mater Civ Eng* 21:110–118. doi:[10.1061/\(ASCE\)0899-1561\(2009\)21:3\(110\)](https://doi.org/10.1061/(ASCE)0899-1561(2009)21:3(110))
- Labuz JF, Zang A (2012) Mohr–Coulomb failure criterion. In: Ulusay R (ed) *The ISRM suggested methods for rock characterization, testing and monitoring: 2007–2014*. Springer, Berlin, pp 227–231
- Li K, Heasley K (2014) Using field measurements to quantify the post-failure behavior of coal. In: *Proceeding of the 49th US rock mechanics/geomechanics symposium*. San Francisco, USA, p 7
- Medhurst TP, Brown ET (1998) A study of the mechanical behaviour of coal for pillar design. *Int J Rock Mech Min Sci* 35:1087–1105. doi:[10.1016/S0148-9062\(98\)00168-5](https://doi.org/10.1016/S0148-9062(98)00168-5)
- Peng S (1986) *Coal mine ground control*, 2nd edn. Wiley, New York
- Peng R, Ju Y, Wang JG et al (2014) Energy dissipation and release during coal failure under conventional triaxial compression. *Rock Mech Rock Eng* 48:509–526. doi:[10.1007/s00603-014-0602-0](https://doi.org/10.1007/s00603-014-0602-0)
- Tutluoğlu L, Öge İF, Karpuz C (2014) Relationship between pre-failure and post-failure mechanical properties of rock material of different origin. *Rock Mech Rock Eng* 48:121–141. doi:[10.1007/s00603-014-0549-1](https://doi.org/10.1007/s00603-014-0549-1)
- Walton G, Arzúa J, Alejano LR, Diederichs MS (2014) A laboratory-testing-based study on the strength, deformability, and dilatancy of carbonate rocks at low confinement. *Rock Mech Rock Eng* 48(3):941–958. doi:[10.1007/s00603-014-0631-8](https://doi.org/10.1007/s00603-014-0631-8)
- Zuo J, Xie H, Wu A, Liu J (2011) Investigation on failure mechanisms and mechanical behaviors of deep coal-rock single body and combined body. *Chin J Rock Mech Eng* 30:84–92